The SAS Seismic Attenuation System for the Advanced LIGO Gravitational Wave Interferometric Detectors

Alberto Stochino [a,b,c,*], Benjamin Abbot [b], Yoichi Aso [d], Alessandro Bertolini [a], Valerio Boschi [a,c], Dennis Coyne [a], Riccardo DeSalvo [a], Carlo Galli [e], Yumei Huang [f], Alex Ivanov [a], Szabolcs Marka [d], David Ottaway [b], Virginio Sannibale [a], Chiara Vanni [e], Hiroaki Yamamoto [a], Sanichiro Yoshida [g]

[a] *LIGO Laboratory, California Institute of Technology, MS 18-34, 1200 E. California Blvd., Pasadena, CA 91125 USA*

[b] *LIGO Laboratory, Massachusetts Institute of Technology, NW 22, 175 Albany Street, Cambridge, MA 02139 USA*

[c] *Dipartimento di Fisica, Università di Pisa, Largo Bruno Pontecorvo 3, 56127 Pisa, Italy*

[d] *Columbia University in the city of New York, 1009 Pupin Laboratory, New York, 10027 NY, USA*

[e] *Galli & Morelli s.r.l. Via Cristofani 558 - loc. Acquacalda 55100 Lucca*

[f] *Department of Astronomy, Beijing Normal University, 100875 Beijing, P.R. of China*

[g] *Department of Chemistry and Physics, SLU 10878, Hammond, LA 70402, USA*

Abstract

Aiming to achieve a significant improvement of sensitivity in the entire frequency range, the forthcoming gravitational wave interferometers of Advanced LIGO have to include new seismic pre-isolation systems. With this objective, the LIGO SAS Group designed seismic attenuation platforms for the HAM and BSC vacuum chambers of the interferometers. HAM-SAS, a prototype designed for the HAM chambers, was constructed and installed in a test bench laboratory. The prototype met or closely approached most of the Advanced LIGO requirements, in terms of seismic isolation, stability and reliability compatibly with the extremely short commissioning time available. In the tests, the system showed the conformity of SAS technology to the LIGO UHV facilities, the structural specs, as well as the ease and safety of the installation procedures. The experience on the HAM-SAS prototype, finalizing the system design, indicated SAS to be a valid option for the seismic isolation in the forthcoming interferometers.

Key words: keyword1, keyword2, keyword3
PACS: code1, code2, code3

1 Introduction

The LIGO interferometers accomplished their task in October 2007 after collecting one year of data at the design sensitivity (S5 science run). A major improvement of the sensitivity is expected from the upgrade of the interferometers to Advanced LIGO [1]. The strain sensitivity [2] should be limited only by fundamental sources of noise in almost the entire frequency range offering a duty cycle higher than the 85% in-lock time achieved by Virgo and LIGO at the end of the S5 science run. This development is expected to yield routine observation of Gravitational Waves. The Initial LIGO interferometers have been mainly limited by seismic noise in the frequency band below 40 Hz [3], leaving a large margin of improvement before the fundamental barrier of the gravity gradients noise at $\backsim$10 Hz is reached.

New seismic pre-isolation systems are needed for the optics tables of both type of vacuum chambers of the interferometers, the Basic Symmetric Chamber (BSC) and the Horizontal Access Module (HAM): the first hosting the main test masses and the beam splitter mirrors, the second containing benches for the input/output optics of the interferometer [5]. The Suspension Systems (SUS) adopted for Advanced LIGO to support the mirrors either hangs from the optics table, as in the BSC [6], or is supported by it from below, as in the HAM [7]. The pre-isolation of the in-vacuum optics tables provides the first level of attenuation of the seismic noise and the low frequency stability needed to acquire and maintain interferometer locking.

Over the last 10 years, the LIGO Seismic Attenuation System (SAS) Group has developed solutions to pre-isolate the suspensions from seismic noise. In view of Advanced LIGO, the group has designed seismic pre-isolation systems for both the HAM and the BSC chambers [8]. We present in this paper the result of the experimental tests carried on a HAM-SAS prototype.

HAM-SAS and BSC-SAS have been motivated by the need of a simple and effective solution to the issue of reliability of the Advanced LIGO isolation platform, alternative to the HEPI-ISI active baseline [9] (see Appendix A for the main points that featured the design). In this perspective, the systems can

* Corresponding Author: *email address*: stochino@ligo.caltech.edu, *mail address* : California Institute of Technology, LIGO Project, 1200 E. California Blvd. 91125, Pasadena, CA USA, MS 18-34, *phone*: +1-626-395-8507.

count on the positive experience on the SAS passive attenuation technology after being largely tested and well proved at Virgo and TAMA [44, 10].

SAS filters are considered passive because most of their attenuation is provided by their mechanical structure, though the performances can be further improved with the assistance of electronic controls. The advantages of seismic passive isolation with respect to active isolation are several. For instance, passive filters are simpler: the isolation comes mainly from the structural elasticity of the materials. This brings many advantages in construction, installation, commissioning and costs. Being effective and stable after initial setup, they are less subject to external unforeseen factors making them more reliable, which is the ultimate factor for high duty cycles of observation science runs. Demanding minimal controls, with low cut-off frequencies and low gain, they are in principle less affected by noise re-injection problems.

The main reason for SAS reliability is its economy of design in which the required attenuation is basically provided by a single and mostly passive stage.

SAS is designed as a primarily passive attenuation unit, with minimally active controls, mainly for static positioning and suspension resonance suppression. Its design resembles that of a large accelerometer's inertial mass. Soft flexures support the payload, while isolating it from the external perturbations. Like in seismometers, the flexures are designed to reach the lowest practical resonance frequencies. The isolation of seismic noise is limited by the flexure material's characteristics (elasticity limit, dissipation characteristics and hysteresis), therefore the SAS response to the seismic noise ideally approaches that of a very sensitive accelerometer.

Passive mechanical filters are at the core of the system. The principle they are based on is that of harmonic oscillators working as low-pass filters for mechanical excitations [12]. Considering one degree of freedom (d.o.f.s) oscillators, the transmissibility, which measures the degree of isolation [1], is flat and unitary up to the resonant frequency. Above the resonance, the displacement of the test mass is progressively reduced with respect to the suspension point and, in an ideal oscillator, it tends to zero as the inverse of the squared frequency.

SAS tackles the problem of the seismic isolation separating the vertical from the horizontal degrees of freedom and studying independent solutions for the two groups. Horizontal and vertical seismic filters are assembled in a way that is intended to minimize the coupling between the two directions, which is one of the main issues in controls of the mass position. SAS design relies on a four-legged Inverted Pendulum table for the isolation in the horizontal plane (two translations and yaw) and a set of four GAS filters in the vertical degrees

[1] The transmissibility represents the transfer function between the position of the suspension point and that of the mass to be isolated.

of freedom (the vertical and the two tilts). The four GAS filters are housed in a rigid "spring box" supported by the IP legs; the spring box moves freely, but uniquely in the horizontal plane. The GAS filters support the HAM optics bench providing free motion in the three vertical d.o.f..

A very important consequence of the choice of soft flexures is the low actuator power requirements. For static positioning the only authority required is that necessary to compensate for tidal movements. For damping and feedback the actuators need only the authority to counter the residual seismic power coupled through the soft flexures. The power dissipated by the actuators is proportional to the square of the force applied [2] that is proportional to the flexure elastic constant times the required excursion. As the elastic constant is proportional to the square of the resonant frequency, 0.2 Hz or lower tuning results in a negligible power requirement [3] . The low power requirements allow the use of simple, safe and highly linear non-contacting actuators [13] as well as low power coil drivers.

Rigid platforms in free motion on fixed modes form an ideal plant for active controls with either or both global interferometer signals feed-back, on-ground seismometer feed-forward or, if sufficient sensitivity is available, on-board accelerometers.

Horizontal LVDT position sensors [14] and co-located voice coil actuators between ground and the spring box, and between the spring box and the optics bench, provide the necessary sensing and actuation for static and dynamic controls.

The solution designed by SAS for the vertical d.o.f.s is the Geometric Anti-Spring filter [42]. The mechanical filter is constituted of cantilever triangular steel blades compressed against a central "keystone" by a supporting disk structure. Under load the blades bend like a fishing rod and work like a linear spring with a very low effective spring constant and thus very low resonant frequency. The effective stiffness depends on the radial compression of the blades: the further the base of the blades is pushed towards the keystone, the softer the response in the vertical direction. A GAS filter with compressions tuned to have a resonant frequency of less than 200 milliHertz can attenuate the amplitude of the oscillation of the load mass with respect to the frame by 3 orders of magnitude (60 dB) above 10 Hz. In the latest version of the filter the attenuation reaches 80 dB by compensating the mass distribution of the blades with an additional device typically referred to as compensation wands [21].

[2] In an electro-magnetic actuator the force is proportional to the coil current I and the dissipated power to I2/R

[3] Micro-Watts for the seismic motion and few milli-Watts for the tidal corrections.

Figure 1. The picture on the left shows a LIGO Horizontal Access Module (HAM) Chamber containing an optics table supported by the LIGO I suspension stacks, which would be replaced by the proposed SAS system without changing the existing optical benches.. The picture on the right depicts a typical LIGO I Basic Symmetric Chamber (BSC).

The horizontal stage is designed around Inverted Pendulums (IP), which can produce attenuation of 100 dB, or more, with the optimized compensation of the center of percussion effect [15].

A prototype of the SAS design for the HAM chamber (HAM-SAS) commissioned by LIGO was built and assembled in Lucca (Italy) by Galli & Morelli Srl. The system was then installed at MIT's LASTI lab to be tested in a LIGO HAM chamber. In this paper we discuss the results obtained from the laboratory tests.

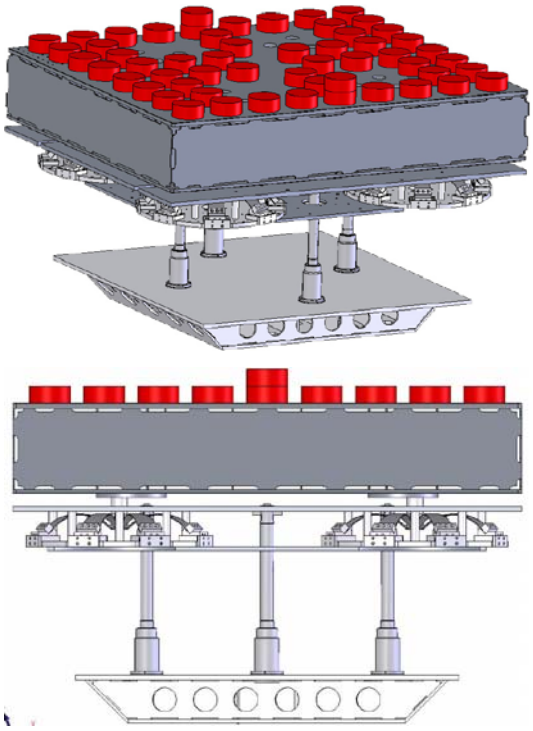

Figure 2. HAM-SAS assembly. From bottom to top: base plate, IP legs, spring box with GAS filters, optics table. The red weights on top represent the actual payload.

2 System's description

HAM-SAS is based on GAS filters and Inverted Pendulums, respectively for the vertical and the horizontal degrees of freedom. Four GAS filters, held together by a rigid cage called "spring box", directly support the optics table. The spring box is supported by four inverted pendulums hinged, to a base plate sitting on the inside of the vacuum chamber.

Each GAS filter is made of 8 maraging steel blades [16], 3.44 mm thick, assembled onto a frame disk of 930 mm diameter [17]. The disks are mounted at the corners of the spring box, constrained between two plates. Stiffening side plates (not shown in figure 2) close the spring box and guarantee its rigidity. The filters simply support the same LIGO-I optics table on spherical tip pins in a quasi-kinematical configuration [18].

The spring box is supported by the IPs. It hangs from the tips of the four IPs' legs (see fig.2), connected by 30 mm long, 3 mm diameter, maraging steel wire joints. The IP legs are 448 mm long light-wall tubes, supported at the base by the main maraging steel flex joints, 50 mm long and 10.5 mm in diameter. Each weighs less than 300 g, including the stiffening overthickness at the two ends. The flex joint at the base and the upper wire joint constitute a double pendulum system supporting the table.

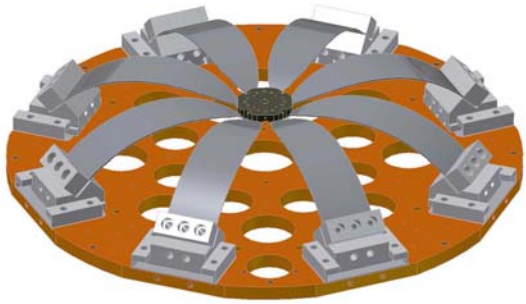

Figure 3. HAM-SAS 8-blade Geometric Anti-Spring (GAS) filter.

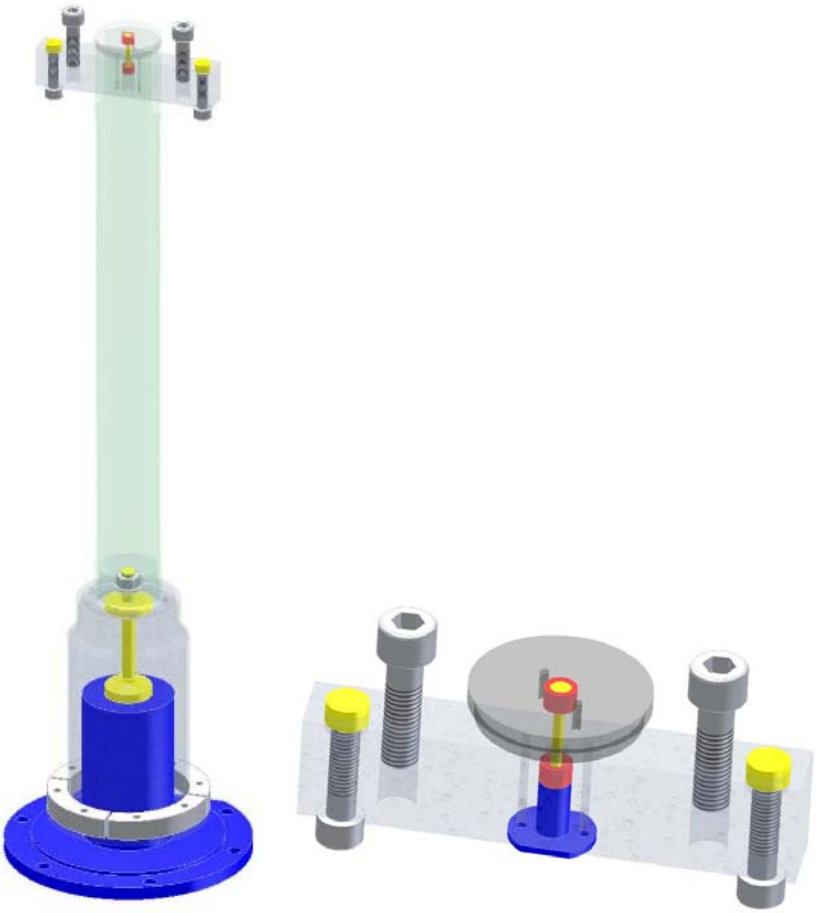

Figure 4. IP double pendulums. We need a 3D picture showing the upper suspension system. 2D va bene, ma dobbiamo espandere il flex joint e mostrare il contrappeso. E' un metodo di sospensione molto sofisticato e importante da spiegare, ma difficile da rappresentare.

Below the main flex point, there is a larger diameter, 174 mm long, leg extension, made to support counterweights for the correction of the Center of Percussion (COP) effect. In IPs this effect arises from the mismatch between the flex point and the rotation point caused at high frequency by the mass distribution in the leg [19]. The consequence is a notch in the transmissibility

	Horizontal LVDT	Vertical LVDT
Deviation from Linearity	0.88%	0.26%
Sensitivity	6.49 V/mm	7.85 V/mm
Range	20 mm	20 mm
Displacement Noise	2 nm/$\sqrt{Hz}$ @ 10 Hz	2 nm/$\sqrt{Hz}$ @ 10 Hz

Table 1
LVDT performances, measured in laboratory bench tests. The deviation form linearity is the local variation of the Position-to-Voltage coefficient across the 20 mm range. The high sensitivity is conserved throughout the range.

at about a few tens of Hertz followed by a plateau where the attenuation stops increasing [15]. An appropriate amount of counterweight below the flex point shifts the COP to overlap the flex point and improves the attenuation. It is SAS experience that well tuned IPs can have attenuation factors of more than 100 dB even with massive legs [20]. The light HAM legs already deliver 80 dB attenuation without COP compensation; therefore a COP compensation at the 10% level is sufficient to yield 100 dB.

The COP effect occurs in GAS filters as well. The effect can be compensated by means of a device, made of a light wand connected by flex joints between the blades' keystone and the frame disk to the blades' base. The wand carries a counterweight and, by changing its position along the shaft, one can introduce the right amount of counteracting momentum of inertia and so reduce the COP effect and improve the filter's attenuation [21, 22]. In HAM-SAS the GAS filters are made to host up to four compensating wands, with one or two of them being sufficient to provide the needed amount of COP correction. The 200 Hz leg's resonances, as well as any other unwanted leg resonance, are damped by a shell of permanent magnets surrounding the IP leg head.

2.1 Sensors and Actuators

HAM-SAS has built-in LVDT position sensors [14]for both stages. Four are located inside the GAS filters and, providing a signal proportional to the height of the filter keystones, measure the optics table's coordinates along the vertical d.o.f.s. Four hang from the spring box, near the IP legs, and measure its position with respect to the base plate and thus the horizontal d.o.f.s. These position sensors are used to provide resonance damping and control feedback to the co-located actuators. The specs obtained by lab measurements on the same LVDTs implemented in HAM-SAS are listed in 1. The displacement noise and total range depend also on the electronics' gain, which can be changed by means of potentiometers in the external readout module.

The design of the system, but not the prototype at MIT, includes also the high sensitivity, UHV compatible, horizontal accelerometers developed by the SAS development group as inertial sensors . Mounted on the spring box, these are immune to the tilts induced by the vertical suspension resonances and movements.

Eight stepper motors, four vertical and four horizontal, apply static offset forces and torques to balance the system and precisely place it in the required position. The first four are mounted on the springs box and connected to the optics table by coil springs, the other four are connected between the spring box and base plate.

In the HAM chambers the optics table and payload are located above the rotation point of the tilts (roughly at the level of the four keystones). This weight distribution introduces a destabilizing torque much stronger than the recall torque from the GAS filters. To solve this problem a cross of four horizontal correction springs has been introduced below the center of tilt to add stiffness on the angular d.o.f.s [18] (see fig. 5) without adding too much to the stiffness in the vertical direction. A vertical shaft is connected to the underside of the optics table, providing the central attachment point for the correction springs while, at the other end, these are connected to the four corners of the spring box. Since the springs are 4-5 cm long, 1 m long thin steel wires are used to cover the distance between the four corners and the shaft. This arrangement introduces a stabilizing torque proportional to the stiffness of the springs used. and a vertical spring constant proportional to their tensioning. The required stabilizing torque can be obtained by choosing the adequate spring stiffness. These springs are minimally tensioned to remain in pull for the entire angular excursion of the table (few mm) while limiting their contribution to the vertical stiffness. The unwanted contribution to the vertical stiffness can be neutralized by adding a small radial compression to some of the blades of the four GAS filters. This compression has to be adjusted according to the height of the payload center of mass to minimize the angular resonant frequency.

3 System Control

3.1 Diagonalization

The number of the sensor/actuator units (four for three degrees of freedom) and their positioning are chosen to match the "rectangular" symmetry of the vacuum chamber, to provide redundancy of sensing and actuation, and to maximize their control efficiency. The coordinates of the optics table are measured with respect to an orthogonal frame referred to the lab. Let $\mathbf{u} =$

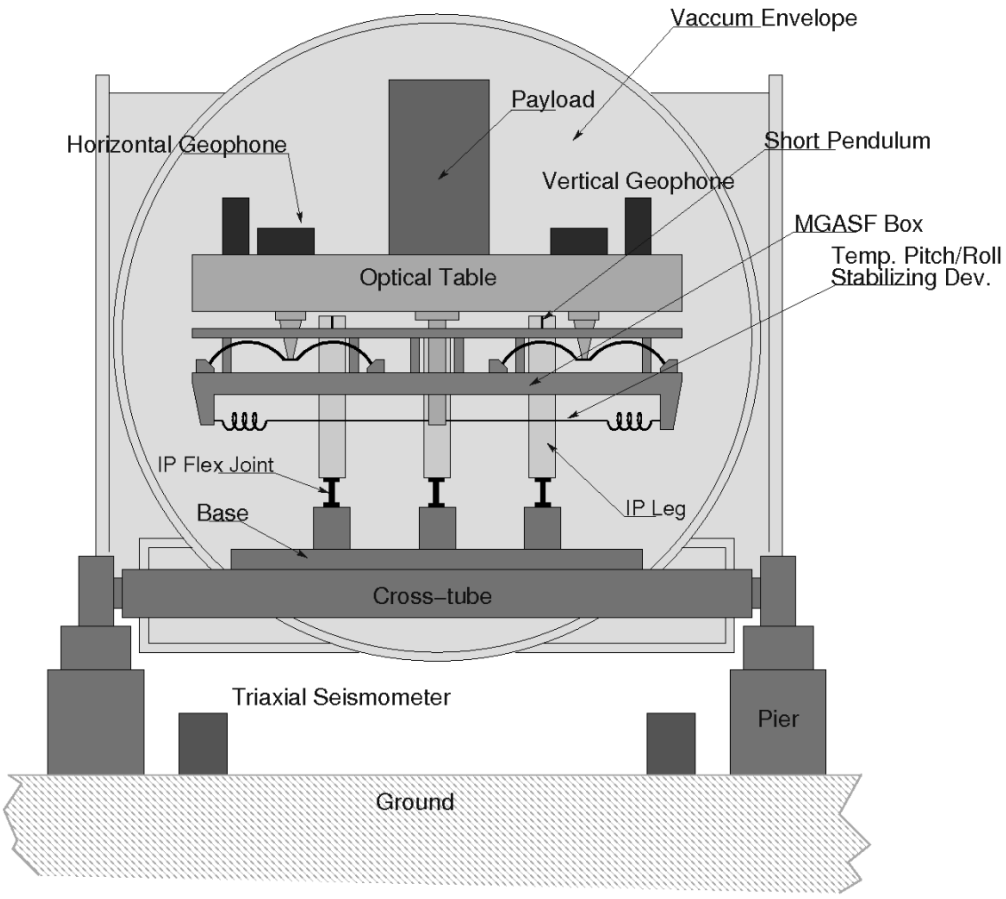

Figure 5. Scheme of the tilt correcting springs added between the top plate and the spring box.

$(h_1, h_2, h_3h_4, v_1, v_2, v_3, v_4)$ be the coordinates from each horizontal and vertical LVDT, and $\mathbf{x} = (x, y, z, \theta_x, \theta_y, \theta_z)$ the coordinates of the geometrical center of the table respect to a Cartesian frame referred to the lab. We have that $\mathbf{x} = U\mathbf{v}$, where U is a 6×8 matrix in the coordinate space that changes the basis. In the same way, for the actuators we can define the vector $\mathbf{v} = (f_{h1}, f_{h2}, f_{h3}, f_{h4}, f_{v1}, f_{v2}, f_{v3}, f_{v4})$, with the forces applied by each coil, and the vector $\mathbf{q} = (q_x, q_y, q_z, q_{\theta x}, q_{\theta y}, q_{\theta z})$, with the total forces and torques applied to the table along the Cartesian coordinates. It is $\mathbf{v} = V\mathbf{q}$, where V is the 6×8 matrix in the space of forces that changes basis. Positions and forces are related by the transfer function of the system that has the form of a 6×6 matrix H, so that $\mathbf{x} = H\mathbf{q}$. The optics table, as a rigid body, has six degrees of freedom and, in first approximation, along each of these, it can be represented by a harmonic oscillator. Six normal modes exist for the overall motion of the system [24].

In general, H is not diagonal, that is each actuator excites all six modes. However H can become diagonal if basis oriented as the normal modes are chosen for $\mathbf{x}$ and $\mathbf{q}$. In the new basis $\mathbf{x}' = S\mathbf{x}$, $\mathbf{q}' = S\mathbf{q}$, where S and D are

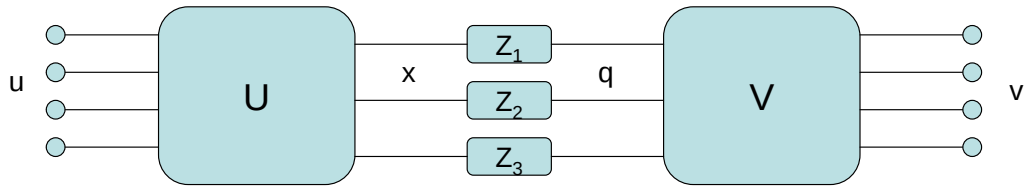

Figure 6. Diagonalization scheme. **u** represents the signals from the four real position sensors for either the horizontal or the vertical degrees of freedom. These are converted into coordinates **x** of virtual sensors by the sensing matrix **S**. Compensation filters **Z** provide the forces **q** to the virtual actuators oriented as the virtual sensors **x**. The virtual forces are projected into real forces **v** on actuator coils by the driving matrix **D**.

usually referred to as sensing and driving matrices respectively, and $\mathbf{x}' = H'\mathbf{q}'$, where the transfer function $H' = SHD^{-1}$ is now diagonal. For this reason, the process is called *diagonalization.*

3.2 Measuring the sensing and the driving matrices

The way me measured H' can be summarized as follows (see [18] for the details). S^{-1} is measured from the relative amplitudes between the sensors' readout in correspondence with each mode. For the driving matrix, one may either directly assume it to be equal to the transpose of S, relying on the fact that the coil actuators are coaxial with the LVDT, or obtain it from the measurements of the ratios $(N)_{ij} = (x_i/v_j)_{\omega=\Omega}$ at a fixed frequency Ω[4]. Since $\mathbf{x} = H'D^{-1}\mathbf{q} \equiv N\mathbf{v}$, $N \propto D^{-1}H'$ is diagonal.

In HAM-SAS the mechanics naturally separates the horizontal and the vertical degrees of freedom. It is therefore useful to separate the modes into two groups (or stages), the vertical and the horizontal, and to consider them as independent from each other. This simplification breaks the problem of the diagonalization into two formally identical ones. H' can be separated in four blocks, with non-null elements only in the two blocks on the diagonal:

$$H' = \begin{bmatrix} [h] & [0] \\ [0] & [v] \end{bmatrix}.$$

If the system behaved completely linearly, we would expect the sensing and the driving matrices to remain constant for all the frequencies. However, non-linearities change the system response and an optimal diagonalization may be frequency dependent for a fully optimized diagonalization.

[4] Ω has to be much lower than any resonant frequency of the modes.

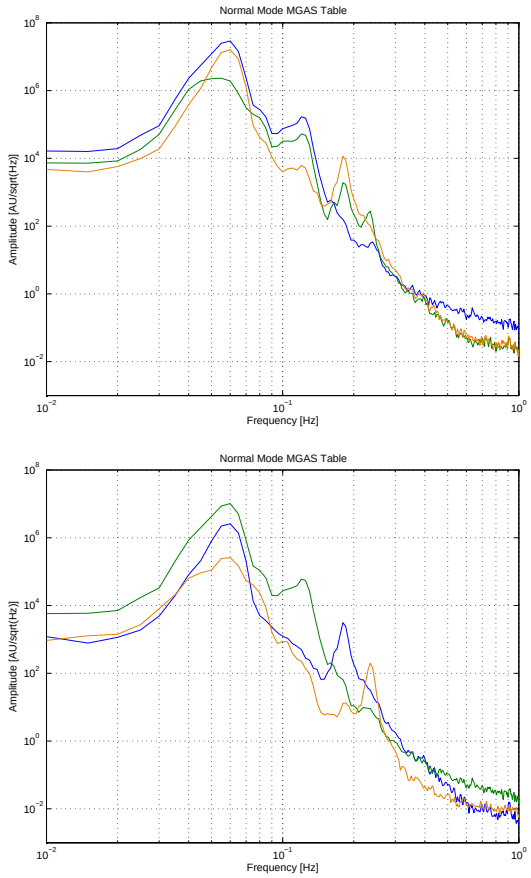

Figure 7. Vertical Diagonalization. The plots show the power spectrum amplitudes of the vertical coordinate signals in the non-diagonalized case (left plot) compared to the corresponding diagonalized sensor signals (right). In the non-diagonalized case all three sensors are equally sensitive to the first two resonances while the third peak is only partially diagonalized. After diagonalization each sensor is only sensitive to a single resonant mode (single peak) with at least a factor of ten rejection of the to unwanted modes. The large resonant peak below 0.1 Hz, visible in all sensors even after diagonalization, is due to yet un-damped horizontal motion coupling into the tilts of the overhanging payload.

4 Physical Plants Transfer Functions

After the diagonalization, the force-to-position transfer function of the system was measured along all the modal coordinates (see 8).

We found the curves matching harmonic oscillator functions with resonant frequencies from 30 to 80 mHz and $Q \backsim 5$ along the horizontal d.o.f.s, and from 150 to 250 mHz and $Q \backsim 10$ along the vertical. These frequencies correspond to the last mechanical tuning before the chamber was closed and the vacuum pumped. Lower frequency values could have been achieved by a finer tuning of the IP load mass, the compression of the GAS blades and an optimization

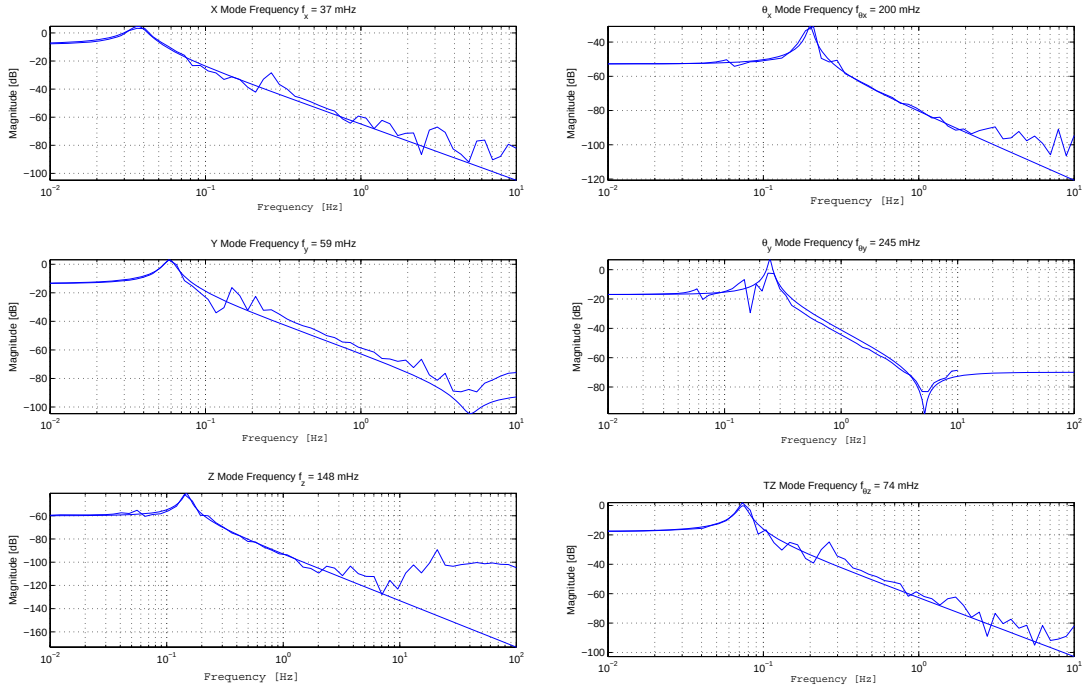

Figure 8. Modal transfer functions of the diagonalized six degrees of freedom. The saturation in Z above 10 Hz is probably connected with the absence of COP compensators.

of the coil springs stabilizing the tilts.

It is in the philosophy of passive isolation to aim to the lowest possible resonant frequencies. The reasons are several:

- the attenuation, proportional to ω^{-2}, starts earlier and then for a same frequency is larger; the actuation force necessary to induce a given displacement in the suspended mass is smaller (proportional to the square of the resonant frequencies);
- the quality factor of each resonance scales with the square of its resonant frequency [12, 15, 18].

Setting Inverted Pendulums and GAS filters to excessively low frequencies leads to instability. Perturbations, due to e.g., vacuum chamber distortion during the pump-down1 can slightly change the balance of the system. For prudence in the first pump-down we decided to leave some safety margin. To compensate we implemented an aggressive control strategy to electronically lower the resonant frequency (EMAS). As doing this is prone to control noise re-injection, the set configuration was far from optimal.

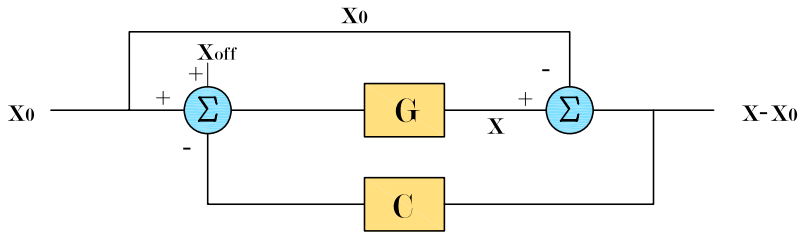

Figure 9. Control topology with relative positions sensors as the LVDTs.

5 Platform Control

In the designed tuning of the system, where low natural frequencies are sought, the role of the control system is minimal, mainly intended to set the mechanical system in its optimal working point and in part also to improve the attenuation performance. The controls can be "passive", based on the LVDTs, which work as relative position sensors, or "active", based on the accelerometer's inertial response, or a combination of both.

The scheme of the passive controls for a single d.o.f. is shown in 9. x_0 represents the reference position (i.e. the ground for the IPs, and the spring box for the GAS filters), whereas x is the corresponding system's coordinate (i.e. the horizontal displacement of the IPs' end or the position of the GAS blades' keystone). G is the transfer function of the mechanical system along the x d.o.f., the so called *physical plant response*, and C is the compensator filter. The closed loop transfer function of the system is:

$$\frac{x_0(\omega)}{x(\omega)} = \frac{G(\omega)\,(1 + C(\omega))}{1 + G(\omega)C(\omega)}. \tag{1}$$

In the active topology, where there is no subtraction of the reference position, the output would be just and the closed loop transfer function would not contain the factor $(1 + C(\omega))$ at the numerator, as in the expression above.

The system prototype at MIT had no built-in accelerometers on the spring box so that the controls that we tested were only the passive ones. We performed some tests to actively control the platform using witness geophones as inertial sensors. Although we did not thoroughly explore this strategy, we closed the loops in all 6 d.o.f., thus indicating the suitability of the actuators and of the plant for inertial controls [25].

In the LASTI tests, which reproduced the conditions of the sites, the controls were implemented by the LIGO Control and Data Systems (CDS) [27, 26]. All the input and output signals were provided by either the ADC or the DAC and the controls were handled by a EPICS digital computer interface. The loop filters were designed in the frequency domain and automatically translated

into the time domain.

Static Position Control.

It is important that the optics table be brought to and maintained at the position required by the interferometer operation. This automatically keeps IPs and GAS filters at their optimal working point if the optical payload is properly positioned. The control loop to maintain the table to an assigned point x_{off} is implemented by an integration filter $C(\omega) = \alpha/\omega$, in which α sets the gain factor, effectively its integration time constant. Assuming $G(\omega)$ is a pure harmonic oscillator transfer function – as we expect it to be if the considered d.o.f. is sufficiently uncoupled from the others – then a necessary criterion for the loop stability imposes that the integration time $\tau = 1/\alpha$ be chosen compatibly to the resonant frequency of the system ω_0, so that $\tau \gg 1/\omega_0$.

Damping Control.

The quality factors of the resonances in the degrees of freedom can be reduced by damping feedback forces, that is by a derivative filter $C(\omega) \backsim i\gamma\omega$.

EMAS

The resonant frequency of a harmonic oscillator can be lowered by introducing an Electromagnetic Anti-Spring (EMAS) in parallel to it [28]. The system is based on a control loop in which the feedback signal is frequency-independent and proportional to the output. The resonant frequency can be lowered or increased by changing the sign of the feedback. Referencing to 9, $C(\omega) = -k$, k being a constant, so that the feedback is positive. Assuming $G(\omega) = \frac{\omega_0^2}{\omega_0^2 - \omega^2}$, according to 1, the closed loop transfer function is

$$G_{cl}(\omega) = \frac{\omega_0^2(1-k)}{\omega_0^2(1-k) - \omega^2} \tag{2}$$

which is the transfer function of an oscillator with an effective resonant frequency reduced by a factor $\sqrt{1-k}$. Care must be used to limit the feedback signals to avoid making the system instable.

With a rough diagonalization, applying anti-springs to a mode affects the others and "drags" their resonant frequencies. When attempting to tune all six modal oscillators to low frequency, the shift of the EMAS in a d.o.f. can destabilize another one. A preliminary test was performed on the vertical degrees of freedom. A rough diagonalization of sensors and actuators was made assuming the modes of the system were a pure vertical translation (z mode) and two rotations along the Cartesian axis of the lab (θ_x and θ_y angular

modes) [5] .

In order not to destabilize the system, we left the two angular modes [6] in their mechanical tuning at 130 and 195 mHz. Static position control loops were applied on the other five d.o.f.s.

We applied the EMAS to drag the vertical resonance down from its mechanical frequency at about150 mHz to about 10 mHz. We traced in Figure 10 the evolution of the vertical resonance as a function of EMAS gain.

To close the EMAS loops on all the d.o.f.s at the same time would demand a fine diagonalization of the system. If this condition does not hold, because of the high EMAS gain necessary to drive the frequencies towards zero, in the mechanical tuning conditions of the present tests, the coils drivers can saturate and even mild seismic excitation may trigger instabilities. We therefore settled for moderate EMAS gains in all three vertical d.o.f., without trying to lower much the resonant frequencies. This kind of control demonstrated to be effective and stable.

The same method can be independently applied in the horizontal d.o.f.s. Low-pass filters could be added in more advanced controls to reduce the EMAS authority at high frequency and prevent noise re-injection from the ground-referred position sensors.

6 Attenuation

The power spectrum amplitude of the residual motion of the optics table and the transmissibilities between ground and the table were measured to characterize the seismic attenuation of the system. The first is measured by three vertical and three horizontal Mark Products L4-C geophones mounted at the periphery of the optics table, roughly in a triangular configuration. The transmissibility is evaluated between three Guralp CMG-T40 seismometers on ground and the six geophones.

The geophones are inertial sensors of relative velocity. Their sensitivity to the displacement is proportional to ω^3 and it is significantly limited at low frequencies, below the internal mass' resonance (about 0.7 Hz). In a more subtle way,

[5] We used the averaged sum of the 4 vertical sensors to generate the vertical feedback signal and sent the same signal in parallel to the four vertical actuators to generate the vertical actuation.

[6] The actual modes of the system turned out to be not very far from these. When we refer to vertical or angular modes in such a Cartesian diagonalization, we mean the modes with the largest vertical projection or one of the angular projections.

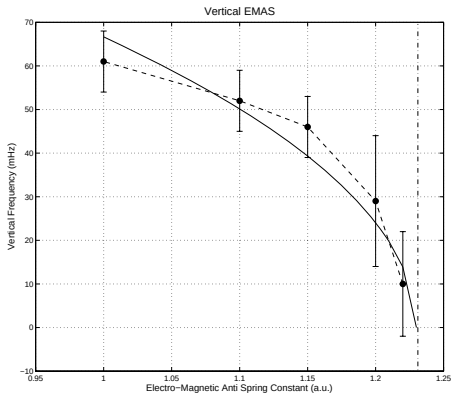

Figure 10. Vertical resonance frequency as a function of EMAS gain. The error bars represent the measured width of each resonance peak. The dashed curve is a square root function fit to the data, its resulting parameters are shown in the box on the left. The vertical dashed line is the critical EMAS gain corresponding to zero recall force.

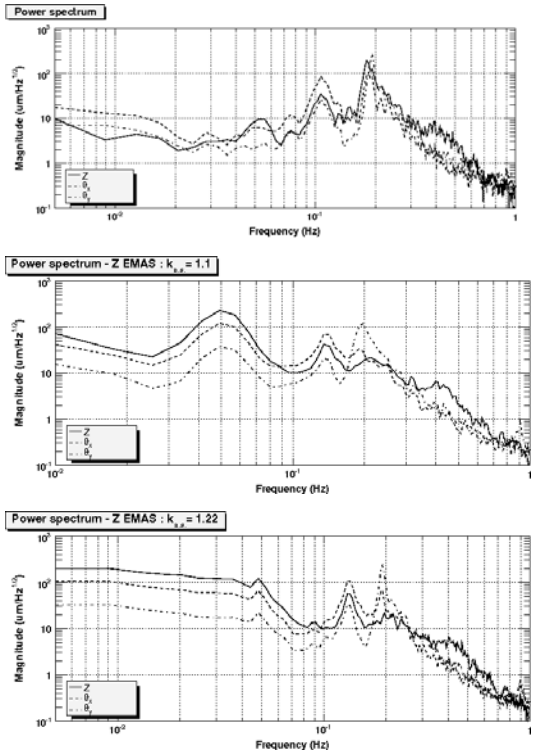

Figure 11. Power spectrum amplitude of the three vertical d.o.f.s according to a Cartesian frame of reference with EMAS control off in the first plot and with EMAS gain =1 (arbitrary units) in the top plot and EMAS gain = 1.22 in the bottom plot. The two peaks at 130 and 195 mHz are the two angular resonances. The peak at 50-60 mHz is the consequence, in the vertical direction, of the un-damped horizontal translation resonances interacting with the overhanging center of mass of the payload. The vertical resonance peak, at 30 mHz for EMAS gain = 1, was tracked in Figure 10, as a function of EMAS gain, as it moved down from 160 mHz and flattened at 5-10 mHz for gain =1.22. The vertical units are LVDT-V/$\sqrt{\text{Hz}}$.

because of the Principle of Equivalence, they are affected at low frequency by tilt-to-horizontal coupling, which prevents them from distinguishing the horizontal accelerations from the angular (θ_x, θ_y). Furthermore, the signal coming out of the L4C electronic driver boards includes a DC component requiring a filter that prevents any significant measurement below 100 mHz.

These considerations about the sensors' limitations allow accurate performance analysis only for frequencies above 100 mHz.

The most important indicator to evaluate the quality of the measurements of transmissibility is the coherence among the sensors. In particular, low values of coherence between the Guralps and the geophones affected the measurements of transmissibility above a few hertz, for the horizontal d.o.f.s, and, above about 20 Hz, for the vertical. Also, the poor coherence among the Guralps themselves prevented the measurement of the ground angular seismic noise, which remains still substantially unknown.

Figure 10 shows the power spectra of the table's residual motion along the laboratory frame, compared with the correspondent seismic ground spectra. The measurements were made with the DC and damping controls on. The straight lines represent the LIGO requirements for the HAM chambers. The measurement mostly meets the requirements except for: the raise to a few $\mu m/\sqrt{Hz}$ at 100 mHz for the vertical direction; a residual peak at about 200 mHz related to the not completely damped vertical modes; the spurious resonance at about 20 Hz due to the wires of the tilt stabilizing springs. These are all minor exceptions, very likely to be overcome with time to optimize the system.

The resonance at 20 Hz can be mechanically damped by tying a cut rubber O-ring halfway along the wires, as successfully demonstrated in laboratory test at. The cut O-ring forms a "C" with an opening and closing frequency much lower than all wire violin modes. The wire violin modes force the "C" to open and close and get efficiently damped by the rubber viscosity. A damping factor of 30 to 100 was observed in a lab test, getting the wire close to critical damping.

The GAS filters need to be tuned at lower frequencies to compensate for the vertical stiffness added by the tilt stabilizing springs, and more tuning mass on the spring box would lower the horizontal frequencies of the IPs below 30 mHz, in the horizontal d.o.f.s. Lower frequency tune would also move the $1/f^2$ attenuation curve to lower frequencies, thus further improving the transmissibility curves.

A natural damping of the vertical resonances would naturally occur with the lower frequency tune as in the design, thus completely eliminating the necessity of control damping.

The transmissibilities in figure 13 show that the attenuation reaches about 70 dB in the horizontal d.o.f.s and 60 dB in the vertical in agreement with measurements performed with a reduced load IP table[7] and with a single GAS filter. Other experiments [15, 18] indicate that at least 20 dB of additional attenuation can be obtained implementing the subsystems for the compensation of the Center of Percussion Effects in both the IPs and GAS Filters[8].

7 Redundancy of the system

Two accidental events during the commissioning revealed some significant aspects of SAS. Once, during installation, the cable of a horizontal actuator was severed. However, the system had enough redundancy and the commissioning was not interrupted, relying on the authority of the remaining three actuators.

In the second accident, the current in one of the actuator, because of a failure in one of the coil drivers, went out of control and started to oscillate rail to rail, dumping its maximum power on the coil. This accident lasted for a few days before being diagnosed but, though the in vacuum coil must have heated up several degrees, it did not significantly over-heat and no outgassing was noticed in the UHV gauges. During the time, the other three actuators acting on the same degrees of freedom under modal control, working against the oscillating one, maintained the table close to its required position, though producing a larger displacement noise on the optics table.

Moreover, once, during the tests the hall air conditioning system failed for a few days. The temperature raised up to 30C. The higher temperature reduced the springs Young's modulus [29], eventually overwhelming the coil actuator authority and moving the table away from its nominal position. The actuators maintained the correct platform assets for a few degrees temperature excursion, much more than the fraction of degree of thermal excursions that can be expected in an observatory experimental hall.

[7] The load was reduced by reducing the flex joint diameter to match the allowable payload of an existing horizontal shaking facility but keeping the same legs later used in the HAM SAS system.

[8] These subsystems, as well as the wire resonance damping O-rings, were not installed during the tests for lack of commissioning time.

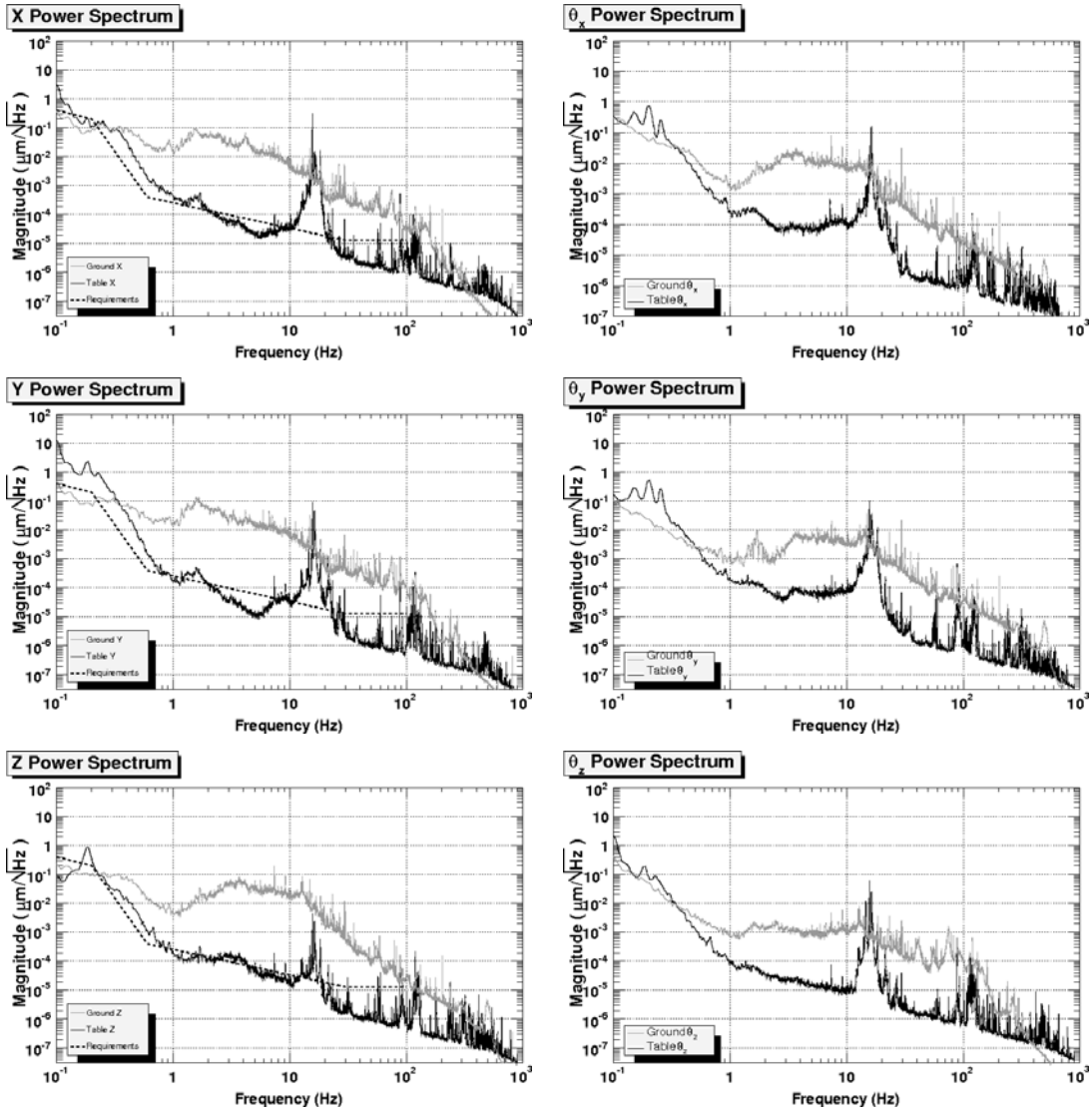

Figure 12. Power spectra. On the left, top to bottom, horizontal d.o.f.s, X, Y, Tz, on the right, vertical d.o.f.s respectively Z, Tx, Ty. The straight line trend of the geophone floor noise above a few Hertz is related to the electronics noise of the sensors and not related to the mechanical performance.

8 Simulations

Modeling and simulation accompanied the design phase of the system and the commissiong of the prototype. A first kind of simulations studied the dependence of the internal modes of the system on the design shapes through Finite Element Modeling (FEA) [31]. The results guided the choice of materials and the configuration of the parts to avoid vibrational modes of the systems at frequencies below 100 Hz. As a matter of fact the test on the prototype showed no significant resonance in the low frequency range due to the individual structure components.

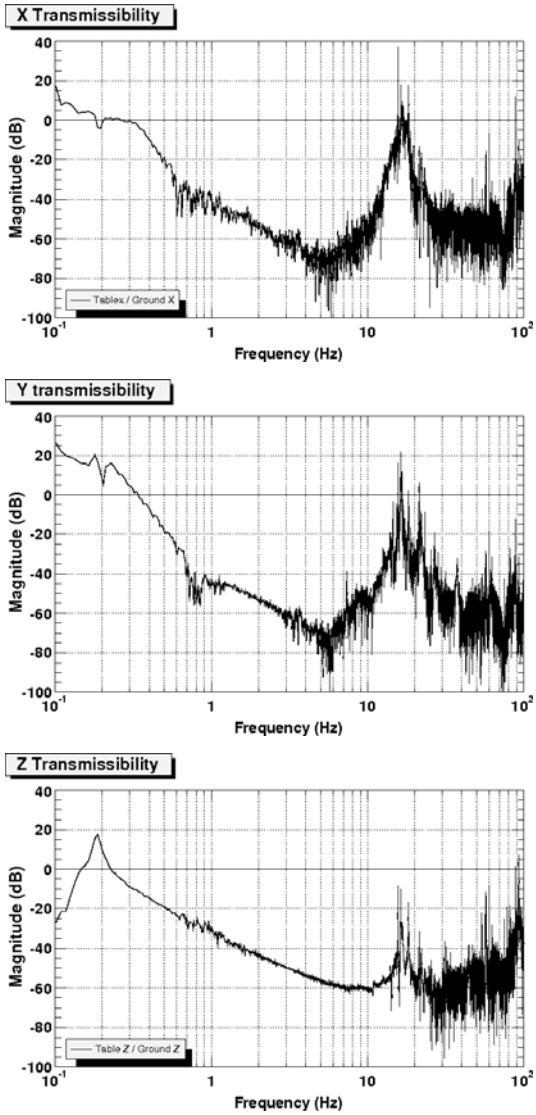

Figure 13. Transmissibilities measured between the Guralp seismometers on ground and the L4-C geophones on the optics table. The peaks between 10 and 20 Hz are due to the undamped wire resonances,

Even though FEM simulations have been useful to study the internal modes of the rigid structure, they were unable to accurately reproduce the dynamic behavior of the complete system, especially at low frequency. A second simulation approach based on multibody dynamics was explored. Two kinds of multibody models have been developed: a linear analytical model written in Maple symbolic language and a non-linear numerical model developed using Multi-Body Dynamics (MBDyn) simulation software [32]. In both models the angular wires' stiffness is neglected and the dissipation mechanisms are accounted using viscous damping to approximate structural/hysteretic damping. These simulations, once validated by confront with the prototype's measured results, provide prediction of the performance for different system tunings. The Maple model showed with appropriate tuning of the IPs' counterweight and

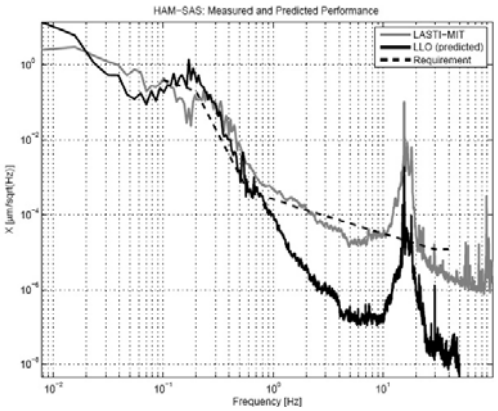

Figure 14. Difference in the horizontal displacement noise between the measurement at LASTI and the prediction with the same transmissibilities measured on the prototype for the seismic noise at the Livingston (Lousiana, USA) interferometer site.

of the GAS blades' COP, more than 100 dB in attenuation can be achieved in the horizontal d.o.f.s and more than 80 dB in the vertical [30]. This model neglects factors like small misalignments of the spring box with respect to the horizontal plane or the uneven balancing of the mass on the optics table and other effects of a not optimal tuning of the system which generate the cross-talk among the d.o.f.s observed in the actual prototype.

An important factor that this model may underestimate is the effect of the angular ground noise for which there are no available direct estimates on site and that the simulations assumed to be correlated to the translational noise [20].

The MBDyn model has the advantage that it can easily include the system intrinsic non-linearities and symmetries. 15 shows the transmissibilities resulting from these simulations compared with the measured ones for the three translational degrees of freedom (X, Y, Z). Since MBDyn analyzes numerically the dynamics of the system in the time domain, the frequency resolution of the simulated transfer function is inversely proportional to the number of seconds calculated (500 s in the plots of figure 17), exactly as in a real measurement. Fitting the model to experimental data provides an estimate of the stiffness matrix of the system and of the compliances between the degrees of freedom. Starting from this we can predict the system performance with different tuning sets. For instance, Figure 15, shows the seismic attenuation improvements when the modal resonant frequencies are further. More than 60 dB are achieved in vertical (still with no GAS Center of Percussion compensation) and more than 100 dB in horizontal.

Regarding the shoulder at 250-300 mHz in the horizontal response graphs, there was no opportunity to fully identify it in the experimental measure-

ments. It may be due to an additional horizontal resonance (due to the GAS angular compliance, or a recoil effect of the tilt modes coupled to the horizontal direction by the overhanging load. In the model we made the "pessimistic" choice to describe it with an additional horizontal resonance. Had we used the recoil description, reducing the resonance frequencies would have further depressed the shoulder and improved the transfer function.

It is also useful to remind that the structure at 15-20 Hz is due to the still undamped wire resonances. Confronting this figure with Figure 12 one notes that the departure above 1 Hz of the measured performance from the simulation in figure 15 may be in part due to the electronics noise of the sensor, which is not far to the measured noise level.

To study the response of the interaction of HAM-SAS with the suspended optics it supports, simulations at a higher complexity level was performed with the use of LIGO's end-to-end (E2E) simulation package [33]. Our particular interest was to assess the degree of the reaction force exerted by the Mode Cleaner (MC) triple suspensions back on the HAM-SAS platform, and to investigate its overall effect on the MC's performance. The E2E MC model consisted of the HAM-SAS component based on the Maple model that simulates the dynamics of HAM-SAS subsystems and the triple suspension component [34] based on M. Barton's Mathematica model [35] that simulates the dynamics of the Mode Cleaner (MC) mirror. The triple suspension's local damping control and the MC cavity's length sensing control were implemented. Accordingly, the back-reaction effects via the local damping and length sensing control actuation forces were considered in addition to the reaction force exerted by the suspension wires via the suspension point. Typical ground translational displacement in the direction of the X-arm was used as input to the HAM-SAS model. The correlation between the ground motions at HAM1 and HAM2 was also considered.

In Figure 16, the effect of the back-reaction via the local damping actuation and the suspension point is assessed through comparison of the MC1 mirror's position motions computed with and without the back-reaction taken into account. In this run, the three MC mirrors were placed at the same locations on the HAM1 and the HAM2 tables as the Initial LIGO detector. Since the MC length control force is applied to MC2 on HAM2, the back-reaction associated with the MC length control is irrelevant in Figure 16. Two cases are shown: with the only horizontal degrees of freedom (dof) of HAM-SAS taken into account (labeled IP) and with both horizontal and vertical dofs taken into account (labeled IP and MGAS). When only the horizontal model is considered, the effect of back-reaction is negligible. However, when the back-reaction for the vertical model is included, the mirror's motion considerably increases in the 1 - 2 Hz range. In particular, the peak at 1.2 Hz becomes prominent, but the noise level still meets the requirement. This frequency is close to the

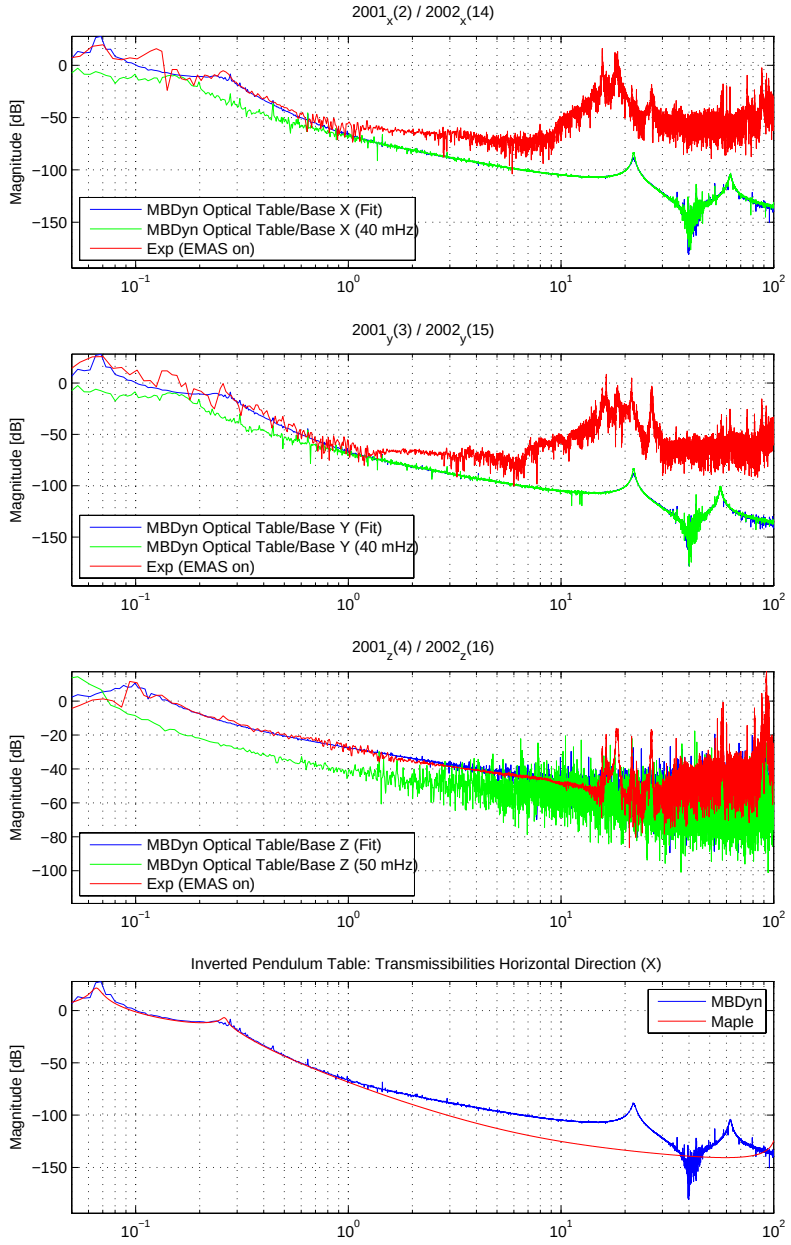

Figure 15. MBDyn model results. The first three plots show how the model (blue line) fits the data (red line) for the transmissibilities of the translational degree of freedom of the system (X, Y, Z, respectively). This allows to estimate the stiffness matrix of the simulated system and from that to extrapolate the transmissibilities with a lower tuning of the modal resonant frequencies. More than 60 dB are achieved in vertical and more than 100 dB in horizontal above 10 Hz. The model also shows the diminishing role of the compliances between the degrees of freedom once that the resonant frequencies are sufficiently low. The Q of the resonance at about 250 mHz, ad hoc included in the model to represent a compliance in the horizontal modes, is reduced when all the rigid body modes are tuned down.

triple suspension's mode #5 resonance (described in [35]) which is dominated by the vertical motions of the middle mass and the lowest mass (the mirror). Figure 16 indicates that the requirements are met from 50 mHz up.

A feedback loop from voice coil vertical inertial sensors, or even from the triple mirror position signal to the table actuators, would counter the back-reaction effect at the lower frequencies and restore the attenuation performance of SAS. This would be useful during lock acquisition, when mirrors are actuated over macroscopic distances. The feasibility of inertial control of the platform was proven during the course of these tests by closing the feedback loop in all six degrees of freedom using the geophones as inertial sensors. As most of the detrimental effect is coupled via the tilts, just the three vertical degrees of freedom would be sufficient to mitigate the recoil effects.

With the E2E simulations it is also possible to predict the frequency noise of the MC transmitted light caused by MC's length fluctuation due to seismic disturbance. Note that this frequency noise is magnified by a factor of 250 (i.e. the ratio of the arm cavity length to the MC cavity length) in the arm cavity [36]. Figure 17 shows the computed frequency noise of the MC transmitted light. When the back-reaction is included, the frequency noise increases in the entire studied frequency range of 0.1 - 10 Hz, peaking at 1.2 Hz. The above-mentioned back-reaction effect on the mirror's motion at 1.2 Hz is responsible for the observed increase in the frequency noise. As a reference, the result of an equivalent computation using the Single Stage LIGO baseline HAM seismic isolation model without the back-reaction effect taken into account is shown.

9 Conclusions

A first unit of SAS has been built, implemented and tested in a LIGO HAM vacuum chamber. Its passive attenuation performance achieved most of the LIGO requirements for HAM chambers, despite the incomplete implementation and tuning due to the very short commissioning time available [36, 37]. The attenuation, with just preliminary tuning and no center of percussion compensation, was such that the measurements were limited in most of the bandwidth by the sensitivity floor of the witness L4C geophones. The results from the simulations indicate that the complete fulfillment of the requirements would come with finer commissioning of the system and implementation of all its subsystems.

The system achieved 60 dB vertical attenuation and 70 dB horizontal attenuation, while 80 dB and 100 dB respectively would be achieved with implementation of the COP subsystems. Lowered normal mode quality factors respectively are expected to be achieved; the tuning of the normal modes to

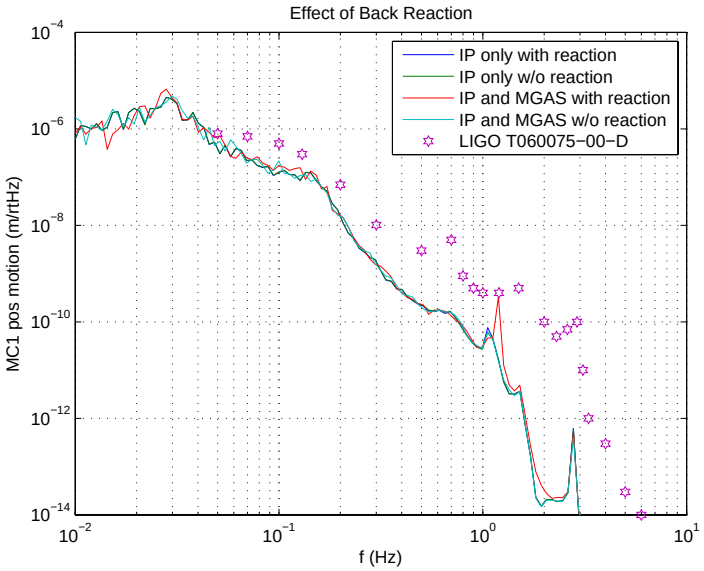

Figure 16. Simulation of the mirror's displacement on a Mode Cleaner (MC) Triple suspension mounted on HAM-SAS including the effect of tilt and translational back--reactions on the platform.

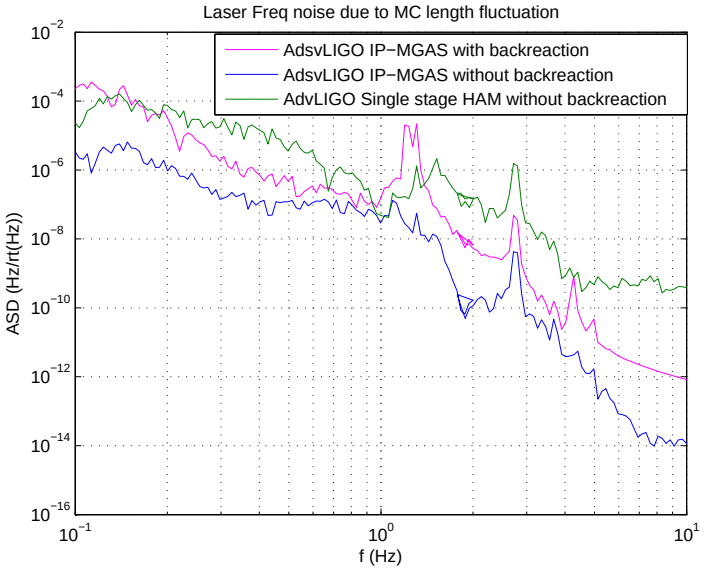

Figure 17. Computed MC transmitted light's frequency noise caused by MC length fluctuation due to seismic disturbance.

lower resonant frequencies would have further damped these modes to the point of making electronic damping unnecessary. Static positioning controls proved effective also against large ambient thermal variations, and would be more than sufficient to compensate for tidal and other seasonal effects.

In terms of vacuum safety and operation reliability, SAS proved performances exceeding the levels accepted for Advanced LIGO (see Appendix A). The

reliability of a mostly passive system, would reasonably reflect in a better duty cycle of the interferometers

Due to the high quality and softness of its flexures, the frequency separation between the SAS rigid body modes and the internal resonances of its structures is very large. Its normal motion modes, and the voice coil actuators are, by design, oriented in the most favorable directions for controls. These characteristics make SAS an good platform for limited-bandwidth optional active controls, as verified by the inertial feedback tests performed using the witness geophone signals.

Only a SAS version for the HAM chambers was realized with only 8 months intervening between construction start and commissioning interruption. It weighs only 700 kg, carrying 1,000 kg of optics bench and payload. A SAS design suitable to instrument the BSC chambers was studied as well. The BSC configuration requires larger GAS filters (one of which has been prototyped in the course of the HAM SAS tests) and longer IP legs, but it is simpler than the HAM version because its optics bench is suspended from wires below the SAS unit and is naturally stable with respect to tilts [38]. Additionally the 0.8 m wire pendulum stage that suspends the optics bench boosts the attenuation performance well above requirements. Apart from these considerations the HAM and BSC SAS design are topologically identical; therefore the results achieved with the HAM prototypes are directly extendible to the BSC case.

The SAS solution was not chosen for the seismic isolation in Advanced LIGO [43]. Based on our commissioning process experience and the measurements performed, we believe that SAS is a viable solution that can be successfully implemented in lieu of the Advanced LIGO baseline. The Virgo experience with the same technology indicates that implementation of SAS would confer higher interferometer reliability and almost unlimited lock time.

Acknowledgements

The authors thank Stan Whitcomb: he understands the problems addressed by this work; without his support the HAM SAS prototype would have never been built. Thanks are also due to Tullio Beneforti, Marcello Berchiolli, Maurizio Caturegli, Robert Laliberte, Myron MacInnis, Stefano Molesti, Mauro Morelli, Damiano Pescallini, Paolo Soldi. Their masterful and enthusiastic technical support made it possible to realize this very difficult project within a very short period of time. Yumei Huang and Ilaria Taurasi also contributed with Finite Element Analysis of mechanical parts. The authors gratefully acknowledge the support of the United States National Science Foundation for

the construction and operation of the LIGO The LIGO Observatories were constructed by the California Institute of Technology and Massachusetts Institute of Technology with funding from the National Science Foundation under cooperative agreement PHY 9210038. The LIGO Laboratory operates under cooperative agreement PHY-0107417.

References

[1] LIGO Scientific Collaboration, ed. P Fritschel, Advanced LIGO Systems Design, LIGO Document T010075-00-D (2001)

[2] Peter R. Saulson, Foundamentals of Inteferometric Gravitational Waves Detector, World Scientific

[3] A. Lazzarini, R. Weiss, LIGO Science Requirement Document, LIGO Document E950018-02 E (1995)

[4] LIGO Scientific Collaboration, LIGO Project System Safety Management Plan, LIGO Document M950046-F, section 3.3.2

[5] Advanced LIGO Team, Advanced LIGO Reference Design, LIGO Document 060056-08-M (2007)

[6] Robertson N.A. and LIGO collaboration, Seismic isolation and suspension systems for Advanced, Gravitational Wave and Particle Astrophysics Detectors, in: Hough J., Sanders G. Eds, proceedings of SPIE, (2004) vol. 5500, pp. 81-91.

[7] Torrie C.I., Development of the suspensions for the GEO 600 gravitational wave detector, PhD thesis, (2000), University of Glasgow.

[8] Bertolini A., R. DeSalvo, C. Galli, G Gennaro, M. Mantovani, S. Marka, V. Sannibale, A. Takamori and C. Torrie, Design and prototype tests of a seismic attenuation system for the advanced-LIGO output mode cleaner, Class. Quantum Grav. 23 (2006) S111–S118

[9] Abbott R. Adhikari R., G. Allen, S. Cowley, E. Daw, D. DeBra, J. Giaime, G. Hammond, M. Hammond, C. Hardham, J. How, W. Hua, W. Johnson, B. Lantz, K. Mason, R. Mittleman, J. Nichol, S. Richman, J. Rollins, D. Shoemaker, G. Stapfer and R. Stebbins, Seismic Isolation for Advanced LIGO, Amaldi Procedings ????

[10] Takahashi R. et al.„ Operational status of TAMA300 with the Seismic Attenuation System (SAS), Proceedings Amaldi 2007????

[11] Takahashi R. et al.„ Control system for the Seismic Attenuation System (SAS) in TAMA300, Proceedings Amaldi 2007 ????

[12] DeSalvo R., Passive, non-linear, mechanical structures for seismic attenuation 5th ASME Int. Conf. on Multibody Systems, Nonlinear Dynamics and Controls (Long Beach, CA, 24-28 Sept.), and references therein (LIGO-P050001-00-D).

[13] Wang C. et al, Constant force actuator for gravitational wave detectors seismic attenuation systems, Nucl. Instrum. Methods A 489 563-9.

[14] Tariq H. et al, The linear variable differential transformer (LVDT) position sensor for gravitational wave interferometer low-frequency controls, Nucl. Instrum. Methods A 489 570-6 .
[15] Raffai P., et al., Inverted Pendulum as Low Frequency Pre-Isolation for Advacned Gravitational Wave Detectors, submitted to LSC.
[16] Braccini S., F. Frasconi, et al., The maraging-steel blades of the Virgo super attenuator, Meas. Sci. Technol. 11 (2000) 467-476.
[17] Gennaro G., HAM Optical Bench, LIGO Documents from D051100-D to D051259-D.
[18] Stochino A., The HAM-SAS Seismic Isolation System for the Advanced LIGO Gravitational Wave Detector, Master Thesis, Univeristy of Pisa, LIGO Document P070083-00-R.
[19] Losurdo G., Ultra-Low Frequency Inverted Pendulum for the VIRGO Test Mass Suspension, PhD. Thesis, Scuola Normale Superiore di Pisa - Classe di Scienze, Italy, October 1998.
[20] Takamori A., et al., Mirror Suspension System for the TAMA SAS, Class. Quantum Grav. **19**, 1615, (2002).
[21] Stochino A., R. De Salvo, Y. Huang, V. Sannibale, Improvement of the seismic noise attenuation performance of the Monolithic Geometric Anti Spring filters for Gravitational Wave Interferometric Detectors, Nucl. Instr & Meth. in Ph. Res. A, 580 (2007) 1559-1564.
[22] Stochino A., Performance Improvement of the Geometric Anti Spring (GAS) Seismic Filter for Gravitational Waves Detectors, SURF-LIGO 2005 Final Report, P050074-00-R.
[23] Bertolini A., High sensitivity accelerometers for gravity experiments, PhD. Thesis, University of Pisa, LIGO Document P010009-00-Z.
[24] Goldstein H., Classical Mechanics, Addison-Wesley.
[25] Stochino A., The HAM-SAS Seismic Isolation System for the Adavanced LIGO Interferometers, Clatech LIGO Seminar Presentation, Pasadena September 4, 2007, LIGO Document ???
[26] Heefner J., LASTI HAM-SAS Digital Controls Requirements and Design Overview, Presentation, Caltech, Pasadena, November 22, 2006, LIGO Document G060596-00-C.
[27] Bork R., LASTI Digital control and Data System Design, February 3, 2006, LIGO Document T060031-00-C (2006).
[28] Mantovani M., R. DeSalvo, One Hertz Seismic Attenuation for Low Frequency Gravitational Waves Interferometers, Nucl. Instr & Meth. in Ph. Res. A, 554 (1-3) (2005) 546.
[29] Verdone N., et al., Extended-time-scale creep measurement on Maraging cantilever blade springs, LIGO Document P070095-00-Z (2007).
[30] Boschi V. et al., AdLIGO HAM-SAS Mechanical Model with Lumped Elements, LIGO Document T060037-00-R (2006).
[31] Boschi V. et al., HAM-SAS Spring Box Simulations, LIGO Document T060066-00-E (2006).
[32] Boschi V., HAM-SAS Mechanics: status of modeling - LSC Meeting,

August 14-17th, 2006 at Louisiana State University, LIGO Document G060445-00-R.
[33] M. Barton, B. Bhawal, M. Evans, H. Yamamoto and S. Yoshida, Simulation tools for future interferometers, Journal of Physics, Conference Series, 32, 398-403 (2006).
[34] Robertson N.A. et al, Advanced LIGO Suspension System Conceptual Design, LIGO Document T010103-05-D (2006).
[35] Barton M., Models of the Advanced LIGO Suspensions in MathematicaTM, LIGO Document T000051-01-D (2005).
[36] Fritschel P., HAM Seismic Isolation Requirements, LIGO Docuement T060075-D-00 (2006).
[37] Ottaway D., HAM SAS Test Plan at LASTI, (2006),LIGO Document T060213-02-R.
[38] Sannibale V. et al., Recent Results of a Seismically Isolated Optical Table Prototype Designed for Advanced LIGO, Proceedings Amaldi 2007, LIGO Document P070127-01-Z.
[39] Majorana E., Mirror Suspension Control VSR1 Learning, LSC-Virgo Meeting at Hannover, October 25, 2007, LIGo Document G070744-00-Z.
[40] Hong Sang Bae, Active Vibration Isolation and Alignment Issues for LIGO, Masters Thesis, Department of Mechanical Engineering, Stanford University, August 1999.
[41] Hua, PhD Thesis ???
[42] Cella G., Sannibale V. et al., Monolithic Geometric Anti-Spring Blades, gr-qc/0406091, NIM A 540 (2005) 502-519.
[43] Shoemaker D., Advanced LIGO HAM Seismic Isolation Technology: Consideration of HAM-SAS as alternative to the baseline design, LIGO Document M070057-00-M.
[44] Acernese F. et al., Virgo: a large interferometer for Gravitational Wave detection started its first scientific run, International Conference on Topics in Astroparticle and Underground Physics (TAUP), Sendai, Japan, September 11-15, 2007.

A Reliability criteria and main features at the base in the SAS design for Advanced LIGO.

The seismic pre-isolation is designed to absorb the variabilities of Earth's crust seismic activity (including anthropogenic noise) and maintain undisturbed interferometer operations. It needs not necessarily to be separated from the rest of attenuation provided by the mirror suspensions. In some other systems (Virgo, TAMA, LCGT, Aciga) the pre-isolation is achieved in an integrated system using the same passive techniques throughout the entire chain.. In

LIGO, the choice of implementing optics benches to support both the main mirror suspensions and ancillary optics has introduced a physical separation between the two stages. The Advanced LIGO baseline solution for the seismic pre-attenuation is the HEPI plus ISI three stage active system containing hundreds of complex sensors and actuators which may lead to a small system time-between-failure. The SAS was designed according to the following tighter reliability criteria.

- The Advanced LIGO pre-attenuation requirements appear to be reachable with a single (mostly) passive attenuation stage.
- Duty cycle. Low frequency, passive pre-isolators proved very effective in isolating the interferometer from external perturbations (human and small earthquakes) potentially enabling longer interferometer locks. (The super-attenuator system allowed Virgo to start its first scientific run with record length locks. The SAS design uses the same, improved technique to provide the same reliability level).
- Instruments' reliability. The entire SAS is designed with passive and completely UHV compatible sensors and actuators, made of polyimide-coated wire wound on Peek spools. The inductive signals are carried outside the vacuum enclosure with twisted pairs and no in-vacuum active circuitry. These instruments, except for physical impact and connector failures, are essentially free of failure modes.
- Vacuum facility risks.
  - No enclosed gas volume is allowed, to eliminate the possibility of virtual leaks hard to identify, for protection of the UHV infrastructure, and for interferometer observational reliability.
  - The assembled and pre-tuned structure is designed for a final Vacuum preparation bake at 120oC, to eliminate the risk of vacuum pollutants accidentally deposited on the parts during assembly.
- Safe actuation power requirements. Low power coils, tolerating indefinite exposure to a railed power supply without out-gassing or damage, are employed. These weak actuators are sufficient to shift or tilt the optics bench as necessary, and provide sufficient authority to cancel the seismic power leaking through the flexures and internal actuation forces (from multiple pendulum actuation), but have insufficient authority to shake it beyond the level of normal seismic activity. Large excursions are achieved by means of static auxiliary springs.
- No standing power allowed. Auxiliary springs attached to stepper motor slides are used to determine the static equilibrium position of the optics table so that no standing forces are required beyond the tidal correction forces and no heat is generated under vacuum. In case of power failure the optics table remains in its equilibrium position without vibrations imposed to the payload.
- Redundancy. Four sensor/actuator units are foreseen for each group of three degrees of freedom, no single sensor or actuator is critical for operation.

Failure of a unit would result in marginally diminished performance not requiring immediate substitution to maintain the interferometer observational reliability.

- Earthquake damage immunity. Already in two occasions the LIGO observatories operations were damaged by nearby earthquakes. The larger Olympia earthquake involved a seismic motion with excursion of almost 5 mm, resulting in the breakage of a suspension and an extended repair period. Advanced LIGO will be even more sensitive to seismic events due to the much higher fragility of the mirror's fused silica fiber suspensions and the small range of their oscillation endstops. A 10 mm range of the low frequency isolation in all degrees of freedom is designed to protect the optics benches from seismic excursions twice as large as the Olympia earthquake. The designed structure is homologous to the Virgo Superattenuators, which suffered a smaller earthquake, with millimetric excursion, with no damage and losing lock only seconds into the seismic event.
- Distant Earthquake immunity. LIGO's locks are interrupted, on an almost daily basis by distant earthquakes. Virgo routinely undergoes these seismic events without losing lock [reference Majorana presentation at LSC in Hannover]. SAS is designed to confer the same seismic immunity to Advanced LIGO.
- Minimized complexity.
  - A single stage, (mostly) passive system is intrinsically simpler than an active system;
  - The six degree of freedom of SAS naturally divide into two virtually-independent, and simpler three d.o.f. groups, which simplifies the controls;
  - Simple and custom design position sensors are used for the static positioning and the other functions of the system. Custom design ensures full control of the functionality and complete knowledge of the instrument, which are often not possible with commercial instruments.
  - The SAS design does not require hydraulic pier pre-isolation.
- Minimized maintenance. No maintenance and no re-tuning are required from a passive system. Although not subject to high stresses, all flexure are baked under load to eliminate any creep-induced change of tune in the experiment lifetime.
- The coil-based, large-stroke position sensors are designed not to require maintenance, and position retuning even for large changes of optics table positioning.
- Payload capacity and payload requirements. The SAS springs are designed with a variable number of blades and dimensioning, to match any desired payload. Similarly the IP flex joint stiffness can be tuned to match the required payload. The payload center of mass must be transversally centered on the system but a payload below the suspension point is ideal and no vertical centering of payload is required. Payload above the suspension point is possible with tilt stabilization springs. This technique, avoiding the necessity of vertical payload centering around the flexures, economizes a large

quantity of ballast mass, making the overall system much lighter and easier to move and handle.

- Tolerances and registering. The structural design and the parts tolerances are compatible with high-temperature bake-out-induced warping. All individual parts, including aluminum parts and coils, are designed to undergo a 200C bakeout, exceeding the required 120oC. Registering is foreseen for all sensitive points to compensate for residual deformations after assembly.
- Rigidity issues.
  - The very low frequency tune of the SAS flexures strongly decouples its supported payload and intermediate rigid platforms from the ground, thus making those platforms ideal for (optional) active controls.
  - The passive attenuation concept of the SAS is the same used in the mirror suspensions it supports. It therefore naturally interfaces with them without the tight rigidity constraints on supported structures typical of active attenuation systems.
- Upgradability. Optional accelerometers are foreseen for performance boosting. They are custom design, fully UHV compatible (no additional vacuum pollution risk) [ref. acc. Bertolini, Barone] with low frequency performance exceeding the best available seismometers.
  - The horizontal accelerometers are positioned on the spring box, ahead of the tilting stage, to mitigate the cradle effect (the Principle of Equivalence causes tilt to be interpreted as an acceleration by the horizontal accelerometers [40]).
  - Even with the accelerometer option, SAS would have less complexity than a single, 6 d.o.f. active attenuation stage because of the mitigation of the cradle effect deriving from the mechanical separation of the horizontal from the vertical d.o.f.s.
- Other possible future upgrades. The pier space is not used by the proposed SAS solution and would remain free for possible future instrumentation.
- Installation: UHV compatible tooling was designed to allow fast, safe and clean installation of the HAM SAS unit and of the optics bench within a working day. The HAM optics bench installs separately, with purely horizontal motion, to allow installation of pre-populated optics benches.
- Costs. SAS simplicity ensures minimized construction, implementation and maintenance costs, both in financial and personnel terms.